Physics – Uspekhi **47** (7) 671 – 686 (2004)

REVIEWS OF TOPICAL PROBLEMS

PACS numbers: **62.50.+p**, **66.20.+d**, 81.30.Bx, **91.35.–x**

Viscosity measurements on metal melts at high pressure and viscosity calculations for the earth's core

V N Mineev, A I Funtikov

DOI: 10.1070/PU2004v047n07ABEH001746

Contents

Abstract. A review is given of experimental and calculated data on the viscosity of iron-based melts on the melting curve. The interest in these data originates in the division of opinion on whether viscosity increases rather moderately or considerably in the high-pressure range. This disagreement is especially pronounced in the interpretation of the values of molten iron and its compounds in the environment of the earth's outer core. The conclusion on a substantial rise in viscosity mostly follows from the universal law, proposed by Brazhkin and Lyapin [1], of viscosity changing along the metal melting curve in the high-pressure range. The review analyzes available experimental and computational data, including the most recent ones. Data on viscosity of metals under shock wave compression in the megabar pressure range are also discussed. It is shown that data on viscosity of metal melts point to a small increase of viscosity on the melting curve. Specifics are discussed of the phase diagram of iron made more complex by the presence of several phase transitions and by the uncertainty in the position of the melting curve in the high-pressure range. Inaccuracies that arise in extrapolating the results of viscosity measurements to the pressure range corresponding to the earth's core environment are pointed out.

V N Mineev, A I Funtikov Institute of Thermal Physics of Extreme States of the Joint Institute for High Temperatures of the Russian Academy of Sciences
ul. Izhorskaya 13/19, 125412 Moscow, Russian Federation
Tel. (7-095) 485 96 66
Fax (7-095) 485 79 90
E-mail: mineev@ihed. ras. ru; funtikov@ihed. ras. ru

Received 1 October 2003, revised 30 January 2004
Uspekhi Fizicheskikh Nauk **174** (7) 727 – 742 (2004)
Translated by V Kisin; edited by A M Semikhatov

1. Introduction

The current understanding of the structure of the earth's core is based on the observation of the propagation of seismic waves that are generated by earthquakes and explosions and travel through internal regions of the earth. Transverse seismic waves are not transmitted through the outer core of the earth, proving that it is liquid. The fact that the earth has a magnetic field, plus some other factors, also confirm that the outer core is liquid. Seismic data also support the view that the inner core is solid [2].

The composition of the core is found by correlating the data on density and bulk modulus of compression with the pressure increase inside the earth. The density distribution with depth was reconstructed from two somewhat differing models that correspond to the ensemble of data on the mass and moment of inertia of the earth and its bulk compressibility corresponding to the velocity of propagation of seismic waves. The pressure inside the earth, determined as the integral of the density times the acceleration of gravity, is calculated quite accurately. The currently accepted Preliminary Reference Earth Model (PREM) [3] gives the pressure at the boundaries of the outer core as 133 and 330 GPa, and that at the center of the earth as 360 GPa (100 GPa = 1 Mbar).

Figure 1 shows the density as a function of the pressure corresponding to the PREM model [3], iron isotherms for $T = 300$ and 5000 K according to [4, 5], and the calculated dependence of the density of iron on temperature in the earth's core (a geotherm) [6].

The earth's core consists of almost 90% iron, while the inner core is made of almost pure iron [7]. The outer core may contain up to 6% nickel and some other light elements (S, O, Si, etc). The presence of these elements (up to 10%) removes the difference between the PREM density distribution curve and the iron geotherm [6]. The density jump at the boundary between the outer and inner cores corresponds to the transition from liquid to solid state and to a change in chemical composition.

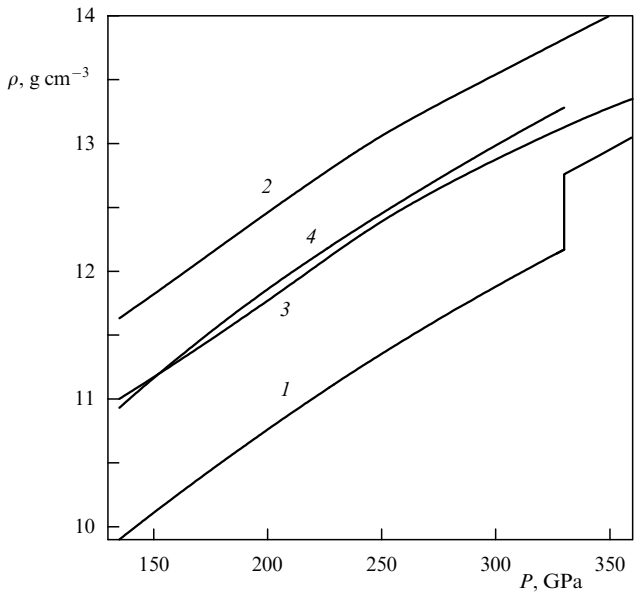

Figure 1. Density as a function of pressure in the earth's core: *1* — according to the PREM model [3], *2*, *3* — on iron's isotherms for $T = 300$ K [4] and 5000 K [5], *4* — on iron's geotherm [6].

The iron melting curve plays the main role in establishing the temperature distribution in the inner regions of the earth. The possibility of molten iron (alloyed with light elements) existing in a limited pressure range is explained in the first approximation by the double intersection of the melting curve on the $T-P$ diagram with the temperature distribution curve in the earth's core. The temperature change at the core–mantle interface is caused by the change in the chemical composition of matter, and hence the melting temperature of iron may be lower in this region than on the geotherm. The temperature distribution in the outer core is a function of depth and is mostly produced by convection; it is therefore very nearly isentropic and corresponds to the situation at the boundary of the inner core. As a result, the melting curve within the outer core may lie somewhat below this isentrope.

The physical properties of iron at high pressures in both the liquid and solid state are the key characteristics for understanding the processes that dominated in the evolution of the earth and other planetary bodies.

In particular, the viscosity of liquid iron, together with the viscosity of iron-based alloys and molten silicates in the earth's outer shell (the mantle), is among the basic parameters for interpreting the seismic data and for justifying the models that explain the chemical differentiation of matter that led to the present state of the earth, as well as the temperature distribution and the generation of the magnetic field.

A recently published review by Brazhkin and Lyapin [1] considered the experimental data and evaluations of viscosity of metallic melts in the high-pressure range and advanced a hypothesis of the universal growth of viscosity on the melting curve accompanying the increasing pressure. These authors came to their conclusions on the basis of the experimental results for iron obtained by one of the authors [8], the available results of viscosity measurements in some liquid metals and melts [9, 10], the analogy with viscosity changing with increasing pressure in a number of organic liquids, and the calculated extrapolation of the data obtained in [1, 8] at pressures less than 10 GPa to a much higher range of values. Brazhkin and Lyapin used the results presented in [1] to predict the increase in viscosity η in the outer core from 10^2 to 10^{11} Pa s with increasing depth and the transition of iron in the inner core of the earth to the glassy state of ultraviscous liquid ($\eta > 10^{11}$ Pa s).

At the same time, the available results of calculations obtained mostly by molecular dynamics techniques [11–14] corresponded to viscosity values $\sim 10^{-2}$ Pa s at the outer core boundaries. Similar values of viscosity were obtained in a number of computational and theoretical papers [15–20] that appeared after the publication of [1].

The experimental results [8, 10] used in [1] are not consistent with the new measurements of the diffusion coefficient [21, 22] and viscosity [23–28] in liquid iron and in liquid melts similar to iron- and sulfur-based compositions. The interpretation of the results of viscosity measurements under shock compression also appears to be incorrect.

The present paper analyzes the available data on the viscosity of iron-based melts in the vicinity of the melting curve and discusses the possibility of extrapolation to the range of high pressure and temperature.

2. Methods of measuring viscosity and the diffusion coefficient

A considerable number of papers were published on measuring the shear viscosity and diffusion coefficient in liquid iron and its compounds with light elements that may be present in the earth's outer core, in the pressure range up to 20 GPa. Three types of measurements are used in such studies:

(1) various modifications of the falling sphere method with viscosity calculated using the Stokes formula;

(2) measurements of the self-diffusion coefficient of iron atoms using radioactive indicators (tracer) techniques, by finding the distribution of an isotope such as ^{57}Fe in the melt after it has cooled;

(3) determination of viscosity by the melt crystallization technique (from crystal grain size).

The essential common feature of all types of measurement is the use of devices that create high pressure in the bulk of the specimen. The specimen must at the same time be uniformly heated to a prescribed temperature in order to eliminate temperature gradients that could drive convective mixing of matter after it has been heated. Such mixing may impede the fall of a ball or distort the evaluated diffusion coefficient. In the first and second methods, such conditions must be maintained for a relatively long period of time [29].

In recent years, the accuracy of directly measured velocities of a ball (typically made of platinum, tungsten or iridium) falling through molten iron or its compounds has been considerably improved in [23–28] by applying the shadow technique of displacement recording. This became possible by using hard X-rays for observing the specimen.

In the Stokes method, viscosity was calculated using the formula

$$\eta = \frac{2wgr^2\Delta\rho}{9V}\,, \tag{1}$$

where r is the radius of the falling ball, V is the fall velocity, g is the acceleration of gravity, $\Delta\rho$ is the difference between the densities of the ball and the specimen, and w is the correction accounting for the difference between the diameters of the ball and the specimen.

Determination of the self-diffusion coefficient by the radioactive indicator technique is based on measuring the concentration of radioactive atoms (^{57}Fe or ^{60}Co) at different distances from the end face of a cylindrical specimen onto which the radioactive marker was deposited [21, 22]. The self-diffusion coefficient D was found from the equation

$$\frac{C}{C_0} = (\pi Dt)^{-1/2} \exp\left(-\frac{x^2}{4Dt}\right) + A(l, x, t)\,, \tag{2}$$

where C/C_0 is the relative concentration of the radioactive component at a distance x from the end face of the specimen, t is the time during which the specimen was maintained in the compressed and heated state, and $A(l, x, t)$ is the corrective function that had to be introduced when the diffusion length $4Dt$ became comparable to the length l of the specimen. The accuracy of the measurements was assured by a long duration of exposure in the liquid state, which was large compared with the times of heating and cooling of the specimen.

The method of evaluating the changes in viscosity on the melting curve, based on finding the average grain size in specimens that crystallized from the melt at different pressures, was introduced in [30]. The effect of pressure on the processes of nucleation and growth of grains in molten iron, lead, copper, and indium was investigated in [8, 31]. As shown in [30], the condition of homogeneous nucleation and growth of crystalline grains is satisfied at high cooling rates ($\mathrm{d}T/\mathrm{d}t > 10^3$ K s^{-1}). The grain size d is related to the effective activation energy that characterizes diffusion and hence melt viscosity as

$$d \approx C\Delta T\left(\frac{\Delta T}{T_\mathrm{m}}\right)^2 \exp\left(-\frac{E_\mathrm{act}}{kT}\right), \tag{3}$$

where C mostly depends on the specimen cooling rate and the melting parameters, $\Delta T = T_\mathrm{m} - T_\mathrm{cr}$ is the overcooling, T_cr is the melt crystallization temperature, and E_act is the effective activation energy. It is assumed that the volume of the critical nucleus is negligible, that is, that the pressure remains constant during crystallization in the entire bulk of the melt and equals the initial pressure.

It was established experimentally that overcooling at a constant pressure is independent of the melt overheating $T - T_\mathrm{m}$ and that if the cooling rate remains constant, the preexponential factor in (3) changes 5 to 10 times less in response to a change in pressure than the exponential [30]. Therefore, the size of grains crystallized from the melt at a small overheating is

$$d \propto \exp\left(-\frac{E_\mathrm{act}}{kT}\right). \tag{4}$$

To obtain viscosity as a function of the temperature and pressure, the formula for the Arrhenius-type activation energy was used in [1, 8], with

$$\eta = \eta_0 \exp\left(\frac{E_\mathrm{act}}{kT}\right), \tag{5}$$

$$E_\mathrm{act} = E_{\mathrm{act}\,0} + PV_\mathrm{act}\,, \tag{6}$$

where $E_{\mathrm{act}\,0}$ is the activation energy at normal pressure and V_act is the activation volume.

Assuming that the melt viscosity at crystallization temperatures close to the melting point is mostly determined by the change in pressure, Brazhkin [8] proposed an approximate dependence of the viscosity on the size of crystalline grains at different pressures,

$$\frac{\eta(P_1)}{\eta(P_2)} \propto \frac{d(P_2)}{d(P_1)}\,, \tag{7}$$

which appears to be applicable in a certain pressure range.

3. Results of viscosity measurements

The main results of viscosity and diffusion coefficient measurements in liquid iron and molten iron alloyed with sulfur as a likely component of the outer core are shown in Table 1. Asterisks mark the data obtained by recomputation of the original measurement results.

The relation between the diffusion coefficient and the viscosity is established by the Stokes – Einstein formula

$$D\eta = \frac{k_\mathrm{B}T}{2\pi a}\,, \tag{8}$$

where k_B is the Boltzmann constant and a is the effective diameter of the atom or the diffusion length. This relation holds for the viscosity and diffusion of simple monatomic liquids [32] but is also valid for molten metals. As shown in [33], relation (8) holds for data obtained at normal pressure in the temperature range above the melting point of metals. In the first approximation, this relation allows comparing the results of independent measurements of viscosity and diffusion.

The applicability of formula (8) to FeS melts at the pressure 5 GPa and temperatures 1300 and 1500 K (which approximately correspond to the conditions under which viscosity and self-diffusion were measured in [10, 22, 27]) was confirmed by first-principle theoretical evaluations [18] obtained by molecular dynamics techniques.

All viscosity data given in Table 1, with the exception of the data of [10], agree with one another and correspond well, via formula (8), to the average values of the measured diffusion coefficients.

Anomalously high values of melt viscosity were obtained in [10] for the molten eutectic $Fe_{73}S_{27}$ in the pressure range of 2 to 5 GPa. The measurements were carried out by the Stokes method, recording the rise of a ball through the melt (a corundum ball of density lower than that of the melt). The velocity of the ball was found indirectly from the change in the resistance between probe electrodes placed on the lateral surface of the specimen. The high values of viscosity in [10] were explained by the authors in terms of the possible polymerization of the melt with increasing pressure, by analogy to polymerization observed in the molecular melt of sulfur. The data of [10] were directly tested in the range of similar states of melt in [24 – 27]. The structural analysis of the $Fe_{73}S_{27}$ melt conducted in [34] found no polymer components at pressures achieved in [10]. First-principle calculations [13, 18] also failed to confirm the formation of such structures under these conditions. Consequently, the results in [10] cannot be explained by the effect of sulfur on the melt viscosity and are interpreted by the authors of other measurements as erroneous. The data may also differ because the ratio of the ball diameter to the specimen diameter in [10] was greater than in other measurements, making them more susceptible to nonuniformities in the temperature distribution, which could result in generation of convective fluxes in the melt.

Table 1. Viscosity and the diffusion coefficient in liquid iron and molten sulfur-bearing iron obtained by various measurement techniques.

Method	Specimen	P, GPa	T, K	D, 10^{-9} m^2 s^{-1}	η, 10^{-2} Pa s	References
Stokes method	Fe	2.7 – 5	1965 – 2093		1.5 – 2.4	[28]
		5 – 7	2026 – 2137		0.4 – 0.9	[28]
		1.6 – 5.5	2050		0.24 – 0.36	[23]
	$Fe_{91.5}S_{8.5}$	2.5 – 6	1823		0.36 – 1.6	[26]
	$Fe_{73}S_{27}$	1.5 – 6.9	1253 – 1821		0.8 – 3.6	[25]
	$Fe_{73}S_{27}$	2 – 5	1373 – 1573		160 – 4360	[10]
	$Fe_{73}S_{27}$	1.5 – 5.5	1423 – 1647		0.7 – 2.2	[27]
	FeS	0.5 – 5	1723 – 1980		0.38 – 1.72	[27]
	$Fe_{61}S_{39}$	5 – 6.9	1333 – 1373		1.6 – 2.4	[24]
Crystallization method	Fe	1 – 4.5	1850 – 1970*	6 – 8**	0.6 – 1.3**	[8]
		5.5 – 9.5	2000 – 2090*	2.3 – 4**		[8]
Method of radioactive indicators	Fe	2 – 20	1883 – 2393	3.6 – 10		[21]
	$Fe_{73}S_{27}$	2.2 – 5	1293 – 1373	1 – 10		[22]

* Estimates obtained in this work.
** Estimates obtained in [21].

The model most widely used to describe the experimentally measured effect of pressure and temperature on the melt viscosity in a limited range of these parameters is the Arrhenius activation model (5), (6), which also corresponds to a similar relation for the diffusion coefficient,

$$D = D_0 \exp\left(-\frac{E_{\text{act}}}{kT}\right). \tag{9}$$

The quasi-lattice approach to describing the properties of and transfer processes in liquids was used by Frenkel and Eyring [35, 36]. The activation volume V_{act} in (6) is assumed to be independent of the pressure. The approximate nature of this approach and the desire to obtain more accurate values of the diffusion coefficient led to creation of a number of computational models. Among them are

- the free-volume model [37], which leads to the dependence $D \propto T^{1/2}$;
- the model based on fluctuation theory (density functional) [38], in which $D \propto T^2$;
- the model of harmonic oscillations of atoms [39], in which $D \propto T$.

The available temperature dependences of viscosity of molten metals were mostly obtained from the Arrhenius relation and differ in the type of the preexponential coefficient in Eqn (5), which may be a function of density and temperature. No advantage was found in using these curves for describing the viscosity data for liquid metals at normal pressure as compared to Arrhenius relation (5).

Because the activation energy is the same for diffusion and viscosity, it follows from Stokes – Einstein formula (8) that in addition to the preexponential factor, Eqn (5) must contain a linear dependence on the temperature. However, the effect of this factor must be small compared to the exponential one [41].

3.1 Iron

The regions in which measurements were conducted in the experiments discussed below are shown in the phase diagram of Fig. 2.

Figure 3 plots viscosity as a function of pressure as reported in [23, 28]. The sharp knee in the narrow zone of pressure change observed in [28] was explained as a possible change in the structure of short-range ordering in the melt, corresponding to the structural transition in the region of solid phases of iron. Indeed, the triple point on the melting curve separating the bcc (δ phase) and fcc (γ phase) structures corresponds to the pressure 5.2 GPa and the temperature 1990 K [44] (see Fig. 2). The change in specific volume in the $\delta \rightarrow \gamma$ transition at the triple point is 1% at the melting points of these phases: 3.6 and 4.6%, respectively [45]. Viscosity

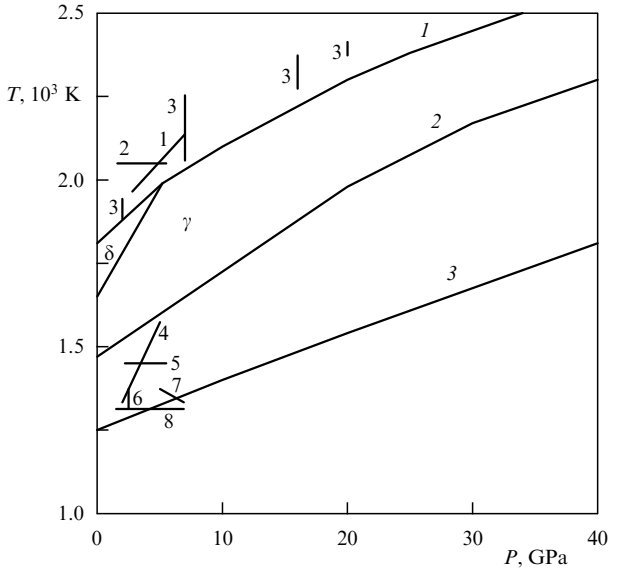

Figure 2. Melting curves and the ranges of measurement of viscosity and the diffusion coefficient. Melting curves: *1* — Fe [6], *2* — FeS [42], *3* — eutectics $Fe_{73}S_{27}$ [43]; measurement ranges: *1* — data [28], *2* — data [23], *3* — data [21], *4* — data [4], *5* — data [27], *6* — data [22], *7* — data [24], *8* — data [25].

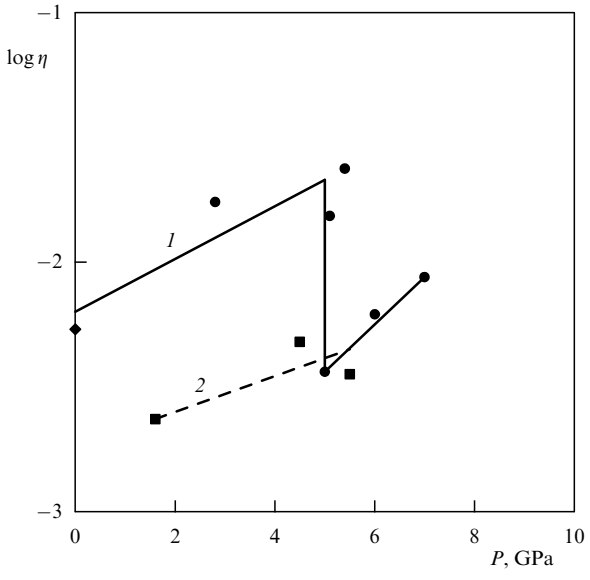

Figure 3. Viscosity (in Pa s) as a function of pressure for liquid iron: *1* — data [28], *2* — data [23]; experimental points: • — data [28], ■ — data [23], ◆ — data [40].

measurements [23] carried out at a fixed temperature of 2050 K are consistent with the data in [28] in the region of the knee. The difference observed in the viscosity value at $P = 1.6$ GPa was probably caused by the increase in overheating $T - T_m$ up to 200 K, which reduced the effect of the initial bcc structure on the structural state of the melt; according to the data in [15], the melt structure corresponded to a denser packing with the coordination number slightly higher than 12. The diffraction measurements carried out in [46] showed the presence of mixed bcc- and fcc-like structures in molten iron at temperatures up to 2300 K in the pressure range from 4 to 5 GPa.

The original viscosity value $\eta = 0.54 \times 10^{-2}$ Pa s for liquid iron (see Fig. 3) corresponds to the generalized measurement results [40], which agree with the data in [33, 47]. The temperature dependence of the iron viscosity at $P = 0.1$ MPa was shown in [40] to depend on the content of impurities in iron and for iron with low impurity content corresponds to the activation energy $E_{act} \sim 2.2$ kJ mole^{-1}. On the other bands, an inflection point was also observed on the curve describing the temperature dependence of viscosity in the temperature range 1850 – 1910 K at normal pressure, which correlated with the change of the melt density and was explained by the near-order restructuring from a δ-like packing to the statistical packing of atoms.

The slopes of the isothermal and isobaric viscosity curves according to Arrhenius formulas (5) and (6) determine the activation volume

$$V_{act} = RT\left(\frac{\partial \ln \eta}{\partial P}\right)_T \qquad (10)$$

and the activation energy

$$E_{act} = R\left[\frac{\partial \ln \eta}{\partial (1/T)}\right]_P . \qquad (11)$$

In calculating the activation energy, the linearized dependence of the viscosity on the parameter $1/T$ is normally used.

It was assumed in [28] that viscosity is mostly affected by pressure. Neglecting the change in temperature within the limits shown in Table 1, the values 4.3 and 7.9 cm^3 mole^{-1} were obtained for V_{act}, using equation (10), for $P < 5$ GPa and $P > 5$ GPa, respectively. It was assumed in [23] that the data of viscosity measurements in the pressure range up to 5 GPa [23 – 28] correspond to a weaker dependence on pressure, namely to $V_{act} = 0.3$ cm^3 mole^{-1} and to 2.8 cm^3 mole^{-1} at higher pressure values. Both these values have considerable errors owing to a small range of pressure variation.

The dependence of the grain size on pressure, obtained for iron along the melting curve in [8], also has a discontinuity at $P \approx 5$ GPa, which corresponds to a change in grain size by a factor of approximately 20. Both regions correspond to nearly linear dependences, for which relation (7) is valid. The separation of the $d(P)$ dependence into two branches was interpreted in [8] as being caused by different values of surface tension of the melt upon crystallization of the δ- and γ- phases.

It must be emphasized that the $d(P)$ dependences obtained in [31] on the melting curve of lead and copper, which do not experience phase transitions in the measurement range, displayed no discontinuities and their slopes were close to the slope of the dependence for iron at a pressure $P > 5$ GPa [8].

The values of the viscosity and diffusion coefficient in molten iron were not determined in [1, 8]. In evaluating changes in viscosity with increasing pressure in the high-pressure phase of iron, it was assumed that by analogy to molecular liquids, V_{act} increases from $0.05V_{act}$ at $P < 1$ GPa to $0.2 - 0.4\ V_{act}$ at $P > 3$ GPa.

The diffusion coefficient was measured in [21] in molten iron using the radioactive tracer method. The concentration of radioactive atoms of ^{57}Fe and ^{60}Co was measured in iron samples along the melting curve in the pressure range from 2 to 20 GPa at temperatures from 1883 to 2393 K (see Fig. 2). The wide range of variation of the pressure and temperature made it possible to compare the obtained data with the results of calculations using the Arrhenius relation and models [37 – 39].

It was found that only the data calculated using the free-volume model and Eqn (9) are close to the experimental data in [21]. Figure 4 gives the results of measurements and the calculated curves obtained with the free-volume model [37] as a function of the parameter $10^3/T$. Only the data of two measurements deviate from the calculations: at $P = 16$ and 20 GPa, corresponding to the maximum values of overheating. The initial value of the diffusion coefficient $D_0 = 12 \times 10^{-9}$ m^2 s^{-1} at normal pressure corresponds to the data in [48]. Curves *6* in Fig. 4 plot the $\log D$ vs $1000/T$ dependence of the diffusion coefficient on the melting curve of iron. The discontinuity on curve *6* also seems to be connected with the phase transition at a pressure ~ 5 GPa.

Figure 5 presents the calculated temperature dependence of the diffusion coefficient along the melting curve of iron according to four models [35 – 39]. We see a significant difference between the curves given by the models in [38, 39], on the one hand, and the Arrhenius curve and the free-volume model curve [37] that are consistent with the measurement results, on the other hand.

Estimates of the diffusion coefficient of liquid iron on the melting curve for the data in [8] were obtained in [21] using Eqn (8). The data in [8], shown by curve *7* in Fig. 4, differ from

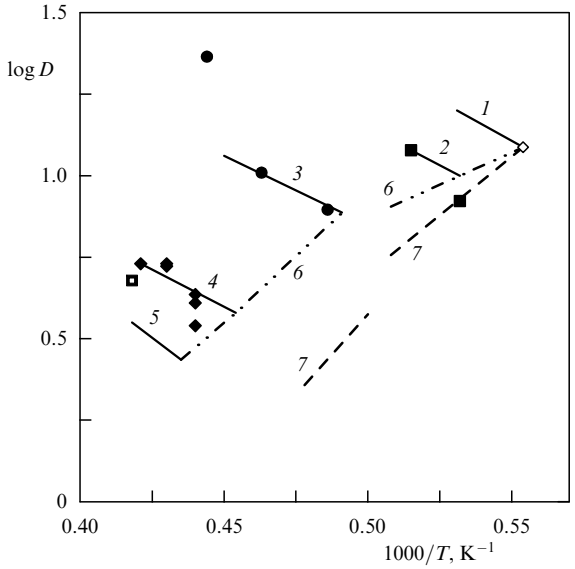

Figure 4. The diffusion coefficient (10^{-9} m^2 s^{-1}) as a function of pressure for iron (according to [2]). Experimental results: ◇ — data from [48] for $P = 0.1$ MPa. ■, •, ◆, □ — data from [21] for $P = 2$, 7, 16, and 20 GPa, respectively; curves *1–5* — free volume model calculations for $P = 0.1$ MPa and $P = 2$, 7, 16, and 20 GPa, respectively, *6* — calculations on the melting curve, *7* — estimates obtained in [21] for the experimental data from [8].

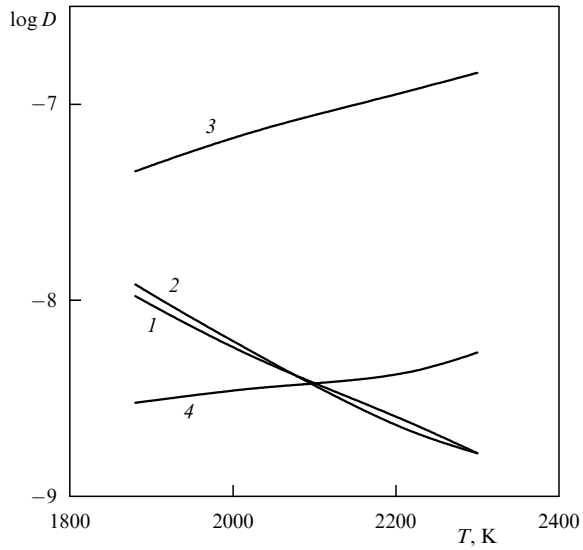

Figure 5. The diffusion coefficient (in m^2 s^{-1}) as a function of temperature on the iron melting curve according to the following models: *1* — Arrhenius relation (9), *2* — free volume model [37], *3* — density functional model [38], *4* — harmonic atomic oscillations model [39].

those in [21], which becomes especially significant for pressures $P > 5$ PGa.

The parameters of the Arrhenius equation for the liquid iron viscosity as a function of pressure at $P > 5$ GPa are given in Table 2. The value $V_{act} = 4.9$ cm^3 mole^{-1} for the data in [8] was calculated using Eqn (7). It appears that the values obtained in [21] are probably more reliable: $V_{act} = 2.8$ cm^3 mole^{-1}, $E_{act\,0} = 120$ kJ mole^{-1}. The excessively large value of V_{act} reported in [28] was caused by inaccurate interpretation of experimental data as a result of using a limited interval of pressure variation and neglecting a slight change in temperature. The value of E_{act} corresponds to the averaged data used in Eqn (6). The Arrhenius curve and the free-volume model [37] can probably be used only within the investigated range of the melting curve of iron; their applicability to higher pressures is discussed in what follows.

Table 2. Parameters of the Arrhenius equation corresponding to measurement results and estimates of viscosity values on the earth's outer core boundaries.

Sample	V_{act}, cm^3 mole^{-1}	$E_{act\,0}$, kJ mole^{-1}	E_{act}, kJ mole^{-1}	$\eta_{135\,GPa}$ 10^{-2} Pa s	$\eta_{330\,GPa}$ 10^{-2} Pa s	References
Fe	4.9*			10^4	$10^{10}-10^{13}$	[2]
	2.8**	120*		1.1***	70***	[21]
	7.9					[28]
	2.8*					[23]
$Fe_{91.5}S_{8.5}$	5.8		260	0.06	1.6	[26]
$Fe_{73}S_{27}$	1.51 – 3.61 4.03****	240 – 405		10^{-4} *****	10^4 *****	[10]
	9.0 4.23****		213 – 252			[22]
	4.28****		100			[27]
	1.5	30				[25]
$Fe_{61}S_{39}$	0.7	40			20	[24]
FeS			255	0.86	1.6	[27]

* Estimates obtained in the present paper.
** Data for $P > 5$ GPa.
*** Estimates for the free-volume model [37].
**** Estimates obtained in [26].
***** Estimates obtained in [22].

3.2 FeS melts

Experimental data on the viscosity of liquid compounds of FeS under varied pressure and temperature are of interest both concerning the state of the earth's outer core and for comparing them with the results obtained for pure iron. Such studies in [22, 24–27] were partly stimulated by checking the anomalous viscosity values of molten FeS reported in [10] and the estimates of iron viscosity in the high-pressure range in [1, 8].

The possibility of the presence of sulfur in the outer core was discussed in [5, 49]. The amount of sulfur that would explain the deficit in density relative to pure iron in the model in [3] and in agreement with the latest data in [49] is expected to be $\sim 7\,\%$ at the boundary of the inner core. The values accepted earlier on the basis of geophysical data pointed to 10–15%; consequently, the parameters of the FeS melt were studied in a sufficiently wide range of sulfur concentrations.

The solubility of sulfur in liquid iron as pressure increases and the effect of pressure on eutectic's parameters in the Fe–FeS system were studied at pressures up to ~ 10 GPa [50]. The eutectic at normal pressure corresponds to the compound $Fe_{73}S_{27}$ and its melting point is 1260 K. As pressure increases, the sulfur content in the eutectic decreases. Calculations in [52] show that at pressures above 130 GPa, the stable compound is Fe–F_3S, corresponding to a sulfur content of 7.5%.

Measurements conducted with diamond anvils at pressures up to 62 GPa established that the melting point of the Fe–FeS eutectic mixture is much lower than the melting point of iron (see Fig. 2). Estimates of the melting point for FeS at higher pressures were made in [52] by temperature measurements at the shockwave front.

Direct measurements of the Fe–FeS melt viscosity as a function of the sulfur content were carried out in [52], where it was shown that $\log \eta$ decreases only weakly as the sulfur content increases. Thus, the viscosity at $P = 2.7$ GPa and $T = 1923$ K decreased from $\eta = 2.7 \times 10^{-2}$ Pa s for pure iron to $\eta = 1.8 \times 10^{-2}$ Pa s for the $Fe_{73}S_{27}$ eutectic [25]. It seems that the value of viscosity reported in [25] corresponds to the minimum level achieved by varying sulfur content in the Fe–FeS melt.

A lower position of the melting curve of the $Fe_{73}S_{27}$ eutectic in comparison with the melting curve of pure iron on the $T-P$ diagram made it possible to reduce the range in which viscosity was to be measured, mostly to the interval 1250–1570 K (see Fig. 2). The measurements were conducted by the same methods as in pure iron. The data of all measurements, with the exception of those in [10] (larger than the results of all other measurements by several orders of magnitude) correspond to values in the range $(0.4-4) \times 10^{-2}$ Pa s (see Table 1). The results of viscosity and diffusion coefficient measurements [10, 22, 24–27] in liquid FeS compounds are plotted in Figs 6–8.

Figure 6 compares the viscosity as a function of pressure in the $Fe_{73}S_{27}$ eutectic reported in [25] for two temperatures, approximately 1310 and 1820 K, with the data in [27] for the compound $Fe_{91.5}S_{8.5}$ [26] at 1823 K, and with the calculations in [18]. In the low-temperature range, a knee is noticeable on curve 1 in the pressure range $\sim 4-5$ GPa, similar to that observed in pure iron (see Fig. 2).

The data in [25, 27] and [10] for the pressure ~ 5 GPa are plotted in Fig. 7 as functions of the parameter $10^3/T$. The deviation of the data in [10] from the measurement results [18, 26, 27] obtained under similar conditions (see Fig. 2) confirms that the results in [10] are incorrect.

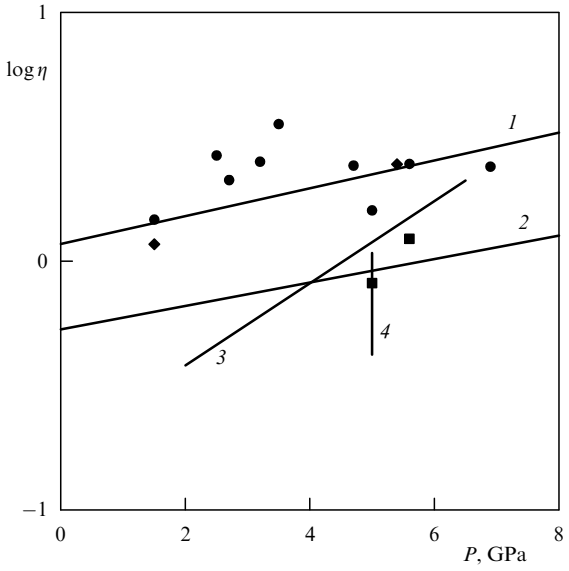

Figure 6. Viscosity (in cPa s) as a function of pressure for various Fe–FeS compounds: *1*, *2* — data [25] for the eutectic at temperatures of 1253–1373 and 1813–1821 K, respectively, *3* — data [26] for $Fe_{91.5}S_{8.5}$ at 1823 K, *4* — calculated results [18] for the eutectic at 1300 and 1500 K. Experimental points: •, ■ — data [25], ◆ — data [27] ($T = 1423-1563$ K).

The behavior of the diffusion coefficient in molten eutectic $Fe_{73}S_{27}$ [22] (Fig. 8) is similar to that observed in pure iron [21].

Table 2 gives the values of the activation volume and activation energy of Fe–FeS compounds, obtained to describe the results of measurements using Eqn (9), as well as estimates of the viscosity corresponding to the parameters at the boundaries of the earth's outer core.

Nearly isothermal curves of the viscosity of the $Fe_{73}S_{27}$ melt as a function of pressure in [24, 25] (see Fig. 6) yielded the values $V_{act} \sim 0.7-1.5$ cm^3 mole^{-1}, which disagree with the

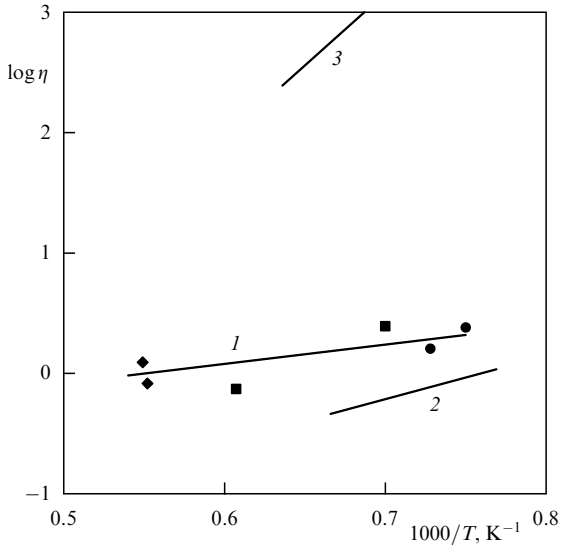

Figure 7. Viscosity (in cPa s) as a function of temperature for the Fe–FeS eutectic: *1* — data [25] for $P = 4.7$ GPa, *2* — calculations [18] for $P = 5$ GPa, *3* — data [10] for $P = 3.9$ and 5 GPa. Experimental points: • — data [24] for $P = 5$ and 6.9 GPa, ■ — data [27] for $P = 2.2$ and 5 GPa, ◆ — data [25] for $P = 4.7$ and 5.6 GPa.

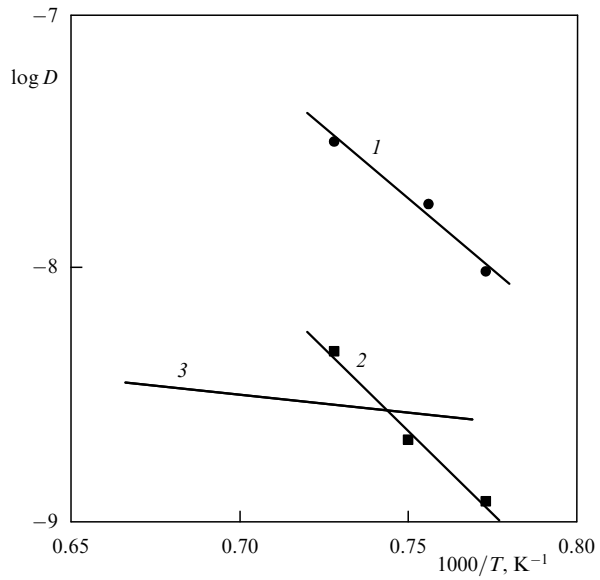

Figure 8. The diffusion coefficient (in $m^2\,s^{-1}$) as a function of temperature for the $Fe_{73}S_{27}$ eutectic. *1*, *2* — data [22] for $P = 2.2$ and 5 GPa, *3* — calculations [18] for $P = 5$ GPa.

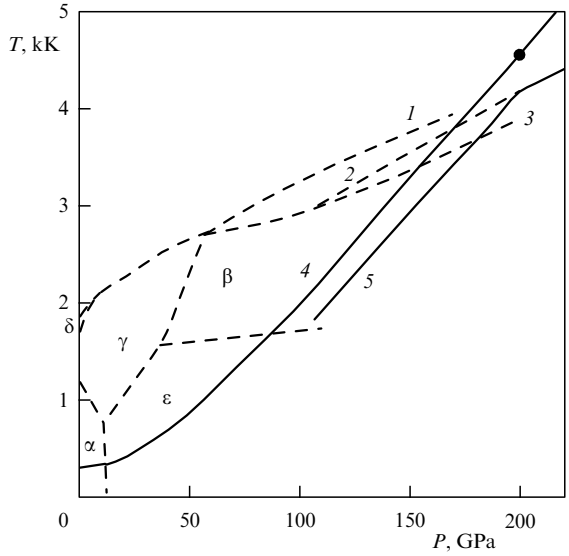

Figure 9. Phase diagram of iron. Dashed curves — phase boundaries and melting curves: *1* — data [60], *2* — data [17], *3* — data [9]. Solid curves — shock adiabats: *4* — data [60] (with melting neglected), *5* — data [17] (with melting taken into account). Black dot: melting on the shock adiabat at $P = 200$ GPa.

value 4.2 $cm^3\,mole^{-1}$ obtained in [26] on the basis of the results reported in [10, 22, 26, 27]. The authors of [26] are of the opinion that this could be caused by making methodological errors of the Stokes method measurements in which the chemical interaction of the ball material with the melt was not eliminated as well as by neglecting certain changes in temperature on quasi-isothermal curves $\eta(P)$. To eliminate the interaction with the melt, a platinum ball in a corundum shell was used in [26]. The viscosity data in [26], as well as the diffusion coefficient curves in [22], yielded the activation energy $E_{act} \sim 250$ kJ $mole^{-1}$.

To clarify the possible cause of discrepancies between the results in [10] and the measurements in [22, 24, 27], calculations were carried out in [18] to evaluate the viscosity and the diffusion coefficient for a liquid Fe – FeS eutectic at the pressure 5 GPa that corresponds to the available experimental data. The first-principle molecular dynamics calculations showed that the viscosity at 1300 and 1500 K was 1.08×10^{-2} and 0.42×10^{-2} Pa, respectively, that is, these values agree with the measurements in [22, 24, 27] and contradict the data in [10]. The calculated diffusion coefficient data ($D \sim 2.5 \times 10^{-9}$ and 3.5×10^{-9} $m^2\,s^{-1}$) roughly correspond to the data in [22]. The calculated results in [18] confirmed the applicability of Eqn (8) under the measurement conditions used for Fe – FeS compounds.

It is thus justifiable, as it was in the case of molten iron, to use the Arrhenius function whose parameters do not differ very much from those for molten iron, to process experimental data on the viscosity of Fe – FeS compounds, despite a certain spread of data, which may originate in methodological measurement errors.

4. Phase diagram of iron in the high-pressure range

Before extrapolating the behavior of viscosity on the melting curve to higher pressures, we consider the available data on the iron melting curve.

Studies of the iron phase diagram and melting curve carried out in the 1990s under conditions of laser heating and static compression in diamond anvil cells covered the pressure range up to 200 GPa and the temperature range up to nearly 4000 K [53, 54]. Melting was detected in this work by a change in the gradient of temperature increase upon heating and by a change in reflectivity of the specimen surface. Novel X-ray-based techniques for diagnosing the in situ status of the specimen greatly helped the studies of the structure of new phases. The measurements showed the presence of another triple point on the iron melting curve (Fig. 9). Subsequent diffraction experiments established that a phase transition in the range of solid phases occurs by transforming the fcc structure to a new β phase identified as the double hexagonal dense packing in [55, 56] or as an orthorhombic structure in [57]. The pressure at the triple point was found to be 60 GPa and the temperature 2800 K [58]. The volume change in the β phase transition was 1.8% [45].

The γ-phase range on the iron phase diagram and, correspondingly, the melting curve of the γ phase are by now determined quite well both for the static conditions [6, 45] and under shock compression [59]. However, the data of static and dynamic measurements begin to diverge at higher pressures. The results of experimental studies of the iron phase diagram and melting curve were analyzed in [6, 60].

Experiments with laser-heated diamond anvil cells showed that transition metals display a general type of behavior, namely a substantial decrease in the temperature growth rate along the melting curve [61]. The slope dT_m/dP_m near the $\gamma - \beta - l$ triple point of the iron γ phase is ~ 4 K GPa^{-1}. As the pressure increases to 200 GPa, the slope of the iron melting curve remains small, $dT_m/dP_m = 7-9$ K GPa^{-1} [6, 53].

At pressures above 200 GPa, the iron melting curve was also found from shockwave data: from measurements of the speed of sound behind the shockwave front [62, 63] and from the temperature measured at the shockwave front [64, 65]. Both sets of data suffer from errors due to inaccuracies in finding the heat terms in the equation of state of iron in the

former case and methodological uncertainty in making corrections to measurement results in the latter.

The sharp drop in the longitudinal elastic speed of sound as a function of pressure behind the shockwave front in iron and the elastic speed of sound tending to the bulk plastic speed of sound were interpreted as attributes of melting on the shock adiabat [62]. According to the data in [63], melting onset corresponds to the pressure 200 – 220 GPa and is completed at $\sim$ 240 GPa.

The data concerning the melting curve found from the knee of the measured temperature curve on the shock adiabat of iron, corresponding to the intersection point of the adiabat and the melting curve, describe behavior in the pressure interval 235 – 300 GPa [65].

The position of the triple point ($\gamma-\beta-1$) as the starting point for the melting curve in the range of higher pressures imposes considerable constraints on the position of the melting curve on the phase diagram, despite the existing uncertainty of experimental data. This factor was used in [60] for evaluating the melting curve using the isentropic expansion of iron from the state on the shock adiabat [66].

Figure 9 plots the iron melting curve [60], the shock adiabat calculated from the semiempirical equation of state with melting neglected [60], and the calculated data [17] taking melting into account. According to the data in [17], melting begins at the pressure 200 GPa and the temperature 4000 K and continues on the shock adiabat up to 280 GPa.

Therefore, the data on the melting curve of iron in the pressure range corresponding to the earth's core and obtained on the basis of static and shockwave measurements are currently incompatible. The discrepancy in temperature at 200 GPa is $\sim$ 800 K [67]. We have no explanation yet for this inconsistency. According to the estimates in [67], the temperatures at the boundaries of the outer core of the earth are 3800 and 5790 K.

5. Calculation of viscosity at high pressures

Two approaches are available for evaluating and interpreting the values of viscosity in the earth's core. Geophysical estimates are obtained by interpreting the data of measurements of the propagation velocity of seismic waves, determining the periods of natural oscillations of the earth and of free nutations of the inner core [7]. Another approach lies in first-principle calculations of shear viscosity in liquid iron and Fe – FeS compounds by molecular dynamics methods using the density functional model. Recent developments in the technique can be found in [11, 12, 14 – 17, 20].

Large values of bulk viscosity are found by calculating the attenuation of radial modes of free oscillations and from propagation of seismic waves [2, 68]. According to the estimates in [19], the bulk viscosity in the outer core must be of the order of $10^6 - 10^{11}$ Pa s and depend on the frequency of oscillations. For instance, the viscosity at 10^{-3} Hz is $10^8 - 10^{11}$ Pa s. The attenuation of longitudinal, so-called P-waves at a frequency $\sim$ 1 Hz in the outer core corresponds to the viscosity $10^6 - 10^9$ Pa s. But the obtained values of viscosity cannot always be made to correspond with the parameters that characterize the physical state of the core or with the position of local regions that correspond to these values of viscosity, and particularly, of the transitional regions at the boundaries of the outer core.

The possibility of a substantial increase in viscosity of the outer core was discussed in [19, 69] in terms of the presence of alloyed components (Ni, S, O), and in [70] in terms of particles suspended in the core. The presence of partially melted local zones in the core was assumed in [71].

The detection of oscillations of the inner core inside the outer core (Slichter modes) made it possible to determine the viscosity in the inner core and in the vicinity of its boundary [72, 73]. The obtained value of viscosity, 1.22×10^{11} Pa s [73], was assigned to the transitional, so-called F-layer at the boundary of the inner core that consists of liquid and solid components. It was assumed that a long-term relaxation of shear stresses that causes the increased viscosity occurs in this layer. However, subsequent studies [74] treated this interpretation of measurement results as ambiguous.

Most of the theoretical models assumed the inner core to be viscoelastic. The Maxwell rheological model was applied to it in view of the value of the effective shear viscosity — from 10^{12} to 10^{17} Pa s [75].

The geophysical estimates of viscosity in the earth's core in the vicinity of the melting curve are inconsistent with the theoretical estimates of viscosity in the liquid state of iron and its alloys given below. It is still important to establish the physical properties of materials, iron first of all, independently of the interpretation of the geophysical information. Frenkel [35], analyzing the viscosity of metals on the melting curve, obtained an estimate of its insignificant variation with increasing pressure and temperature, namely, $10^{-3} - 10^{-2}$ Pa s for the outer core environment.

Numerical evaluations of the bulk and shear viscosity by methods of molecular dynamics have recently achieved considerable progress; the main difference lies in the approaches to describing the electron state. The technique was initially used for determining structural parameters and the density of solid phases of iron and later its melting curve in the high-pressure range as well [17, 20, 76, 77].

Calculations of the shear viscosity and diffusion coefficients of liquid iron were carried out for the pressures and temperatures that correspond to the outer and inner boundaries of the outer core. Different calculations used somewhat different values of temperature in the ranges 3970 – 4300 and 5400 – 6000 K in order to arrive at the density and pressure close to the parameters of the PREM model [3]. Figure 9 demonstrates that these values of temperature at the core – mantle interface fall above the iron melting curves, that is, they point to overheating by $\sim$ 700 – 800 K. As we mentioned above, temperatures at the boundary of the inner core appear to be closer to the data on the melting curve.

Calculations assumed that the viscosity mechanism of iron in the outer core remains the same as in the already investigated range of not very high pressures.

Table 3 gives the pressure, density, diffusion coefficient, and shear viscosity of liquid iron calculated by molecular dynamics techniques in the papers listed in column 6. The viscosity at the core boundaries was found to be $(0.9 - 1.2) \times 10^{-2}$ and $(1.3 - 3.3) \times 10^{-2}$ Pa s; these values are in good agreement with earlier numerical results [78 – 80] and with scaling estimates [33] for liquid iron (Table 4). The data for iron in [15] were obtained with an improved computational technique and differ from earlier results by the same authors [81] that gave too high values of the iron viscosity, $\sim 90 \times 10^{-2}$ Pa s for the conditions in the outer core, which exceeds the viscosity of simple liquid metals by an order of magnitude.

Table 3. The pressure, temperature, density, diffusion coefficient and shear viscosity of liquid iron corresponding to states at the boundaries of the earth's outer core.

P, GPa	T, K	ρ, g cm^{-3}	D, 10^{-9} m^2 s^{-1}	η, 10^{-2} Pa s	References
135	4300	10.70	5		[11]
135	4300	10.70	4	1.2	[12]
132	4300	10.70	5.2	0.85	[15]
132	4300	10.70	5.8		[20]
360	6000	13.30	5	1.5	[15]
330	6000	13.30	5	1.3	[12]
330	6000	13.30	4 – 5	2.6 – 3	[11]
330	5400	12.80		1.3	[17]
358	6000	13.60	3.2		[20]

Table 4. Shear viscosity (10^{-2} Pa s) of liquid iron corresponding to pressures at the boundaries of the earth's outer core.

Author, year	$P = 130$ GPa	$P = 330$ GPa
Gans, 1972 [78]	0.37	1.85
Poirier, 1988 [33]	0.3	0.6
Svendsen et al., 1989 [79]	0.9	1.4
Stixrude et al., 1998 [80]		0.5

The calculated estimates of the viscosity of molten iron alloyed with 12% sulfur at the boundary of the inner core ($T = 6000$ K, $\rho = 12.33$ g cm^{-3}) were reported in [14]. The obtained value $\eta = 1.3 \times 10^{-2}$ Pa s was quite close to the data in [11, 12].

Molecular dynamics techniques, similar to those used in [16 – 18], seem to have been used for the first time in [11, 15] for independent calculations of the bulk and shear viscosity. As in the case of the data given above, the calculated values of the density of liquid iron at the boundaries of the outer core are in good agreement with those for iron alloyed with 10% nickel, and also with the data in [3]. These results are listed in Table 5. It was observed that the bulk viscosity of the alloy roughly corresponds to that of iron. Hence, the presence of nickel in the outer core can reduce the bulk viscosity of the melt only slightly. According to the calculations for iron and the alloy, the relation $\eta_v = 0.12\eta_s$ holds in the entire range of pressures and temperatures. The shear viscosity was $\sim 10^{-2}$ Pa s, as in earlier calculations for these conditions.

We also note that iron and its alloys with nickel demonstrate a similarity in other parameters. The differences in the isothermal compressibility between iron and the alloy (the experimental data in [4]) at normal temperature at pressures up to 300 GPa were less than 1.5%. The melting curve for the iron – nickel alloy above 60 GPa also appears to be close to the iron melting curve [82].

Table 5. The pressure, temperature, density, diffusion coefficient, and shear and bulk viscosity of liquid iron and liquid alloy Fe_{90} Ni_{10}, corresponding to the states at the boundaries of the earth's outer core.

M	P, GPa	T, K	ρ, g cm^{-3}	D, 10^{-9} m^2 s^{-1}	η_s, 10^{-2} Pa s	η_v, 10^{-2} Pa s	References
Fe	135	3970	10.37	3.2	1.2	0.32	[16]
	330	5950	12.51	1.87	3.3	0.32	[16]
$Fe_{90}Ni_{10}$	133	3961	10.37			0.1	[19]
	330	5975	12.54			0.34	[19]

The values of viscosity at the boundaries of the outer core yielded by approximate numerical models discussed above are listed in Table 2.

Estimates generated in [21] using the free-volume model [37] for the pressure 130 GPa and temperature 4300 K corresponded to $D = 2.5 \times 10^{-9}$ m^2 s^{-1} and $\eta = 1.1 \times 10^{-2}$ Pa s. These values are sufficiently close to the numerical results in [15] obtained by molecular dynamics techniques: 5.2×10^{-9} m^2 s^{-1} and 0.85×10^{-2} Pa s. But they are too high as far as the vicinity of the inner core boundary is concerned ($P = 330$ GPa, $T = 6000$ K). Estimates of the diffusion coefficient using the Arrhenius relation in [21] yielded substantially larger deviations (by 10 – 20 orders of magnitude), for instance, in comparison with the data in [15]. A similar extrapolation of viscosity using the Arrhenius relation in [10, 22 – 28] also gives greatly overestimated and unreliable results.

With the dependence of $V_{\rm act}$ on the pressure along the melting curve assumed in the form $V_{\rm act} \sim 1/\rho$ for the modified Arrhenius model, the viscosity at the boundaries of the outer core was estimated to be between $\eta \approx 10^4$ and $10^{10} - 10^{13}$ Pa s (see Table 2). According to the evaluation in [21], the corresponding values of the diffusion coefficient are 1.2×10^{-8} and 9.2×10^{-15} m^2 s^{-1}. These results remain considerably lower than those obtained with the free-volume model.

The reason for the fast growth of metallic melt viscosity along melting curves consists, in the opinion of the authors of [1], in a steeper dependence of pressure on density as compared with the dependence of the melting point on density. For the melting curve, it was assumed in [1] that

$$P \propto \rho^{4-5} . \tag{12}$$

In reality, this function, usually represented in the form

$$P = K_{S0}\left[1 + \left(\frac{\rho}{\rho_0}\right)^{K'}\right], \tag{13}$$

where K_{S0} is the initial value of the modulus $K_S = \rho(\mathrm{d}P/\mathrm{d}\rho)_S$ for $\rho = \rho_0$ and $K' = \mathrm{d}K/\mathrm{d}P$, corresponds to the 300 K isotherm. The measurement data for iron obtained in [4] correspond to $K' = 4.81$ [83].

The variation of density along the melting curve can be calculated using the semiempirical Mie – Gruneisen equation of state with separation of cold (elastic) and thermal components of pressure and energy,

$$P = P_{\rm c} + P_{\rm t}\,, \quad E = E_{\rm c} + E_{\rm t}\,. \tag{14}$$

Equation (13) was used in [60] to describe the cold components of the equation of state in iron; for thermal components, the equation

$$P_{\rm t} = \gamma\rho E_{\rm t}\,, \quad E_{\rm t} = C_V(T - T_0)\,, \tag{15}$$

was used, where γ is the Gruneisen coefficient, $T_0 = 300$ K, and C_V is the heat capacity. In the approximation where $\gamma\rho = \text{const}$, using the Lindemann relation

$$\frac{\mathrm{d}\ln T_{\rm m}}{\mathrm{d}\ln\rho} = 2\left(\frac{\gamma - 1}{3}\right) \tag{16}$$

allows relating the melting point to the density as [84]

$$\frac{T_{\rm m}}{T_{\rm m0}} = \left(\frac{\rho}{\rho_{\rm m0}}\right)^{2/3} \exp\left[2\gamma_{\rm m0}\left(1-\frac{\rho}{\rho_{\rm m0}}\right)\right], \qquad (17)$$

where $T_{\rm m0}$, $\rho_{\rm m0}$, and $\gamma_{\rm m0}$ are the initial values of the parameters.

The choice of values of $\gamma\rho$ in [60] made it possible to describe melting curves in the region of γ and β phases of iron. The lower-slope melting curve of the γ phase corresponded to the value $\gamma\rho = 9.5$ g cm^{-3}, and the steeper-slope one to $\gamma\rho = 13.5$ g cm^{-3}. The shockwave data on the melting curve in the range $P > 200$ GPa correspond to still a greater value of $\gamma\rho$. In this case, the function $T_{\rm m}(P_{\rm m})$ must approach a linear form. We note that Boehler's initial measurements of melting curves in the $100 < P < 200$ GPa range recorded a melting curve of iron with the constant slope $\mathrm{d}T_{\rm m}/\mathrm{d}P_{\rm m} = 9.5$ K GPa^{-1} [53].

In terms of the Arrhenius activation model, with

$$\eta = \eta_0 \exp\left(\frac{E_{\rm act\,0}}{RT_{\rm m}}\right) \exp\left(\frac{V_{\rm act}P_{\rm m}}{RT_{\rm m}}\right), \qquad (18)$$

the linear or even faster (unrealistic) growth of the temperature on the melting curve, that is, the case where $\mathrm{d}^2T_{\rm m}/\mathrm{d}^2P_{\rm m} \geqslant 0$, must result in a decrease of the viscosity with increasing the pressure; in the opposite case, represented by the data for iron, the viscosity must increase along the melting curve.

Indeed, according to the equation of state in [60], the viscosity in the region of the γ phase increases with increasing the pressure up to 0.4 Pa s and continues to grow. As in the case of the $\delta - \gamma - 1$ triple point, we can expect the density change on the melting curve at the $\gamma - \beta - 1$ triple point to result in some decrease in viscosity. However, the applicability of the Arrhenius model in the high-pressure range can be rejected according to the numerical and theoretical data given above.

The viscosity of iron in the states typical of the earth's outer core is thus better justified in the theoretical calculations considered above than in the extrapolated estimates that follow from experimental results at not very high pressures. The calculated value of viscosity in liquid iron is $\sim (1-1.5) \times 10^{-2}$ Pa s, which corresponds to an insignificant increase in viscosity on the melting curve. Adding nickel and sulfur to iron does not increase the viscosity. Clarifying the nature of low viscosity in the outer core is important for understanding the processes of circulation and convective heat exchange in the outer core. The interpretation of high viscosity is related to the possible existence of partially melted systems and suspensions inside and at the boundaries of the earth's core.

6. Viscosity measurements in shock compression

Compression of matter by shock waves makes it possible to achieve pressures of dozens and hundreds of GPa, far beyond the capabilities of static methods [85]. The parameters of the compressed material, including its viscosity, are determined by processes that accompany shock compression: high-rate straining of matter at the shockwave front, its nonadiabatic heating, and the displacement of material behind the shockwave front. We note that the viscosity of matter affects both the width of the shockwave front and the rate of dissipative processes involved in the shock wave propagation. Therefore, the dependence of viscosity on shockwave intensity is by no means straightforward.

Because the results of shockwave experiments on viscosity measurements in aluminum, iron, lead, mercury, and water in the megabar pressure range [86–90] were interpreted in [1] as pointing to an increase in viscosity by several orders of magnitude, these results must be considered in more detail.

The physical picture of high-speed shockwave deformation of an initially solid matter is quite complicated owing to the rheological properties of materials under shock compression [91]. The manifestations of viscosity in material flow corresponding to a counteraction due to the velocity gradient is analogous to diffusion processes involving transport of particles and leveling of the composition in the presence of concentration gradients. The value of viscosity is determined not only by thermodynamic parameters but also by the deformation rate. Depending on the type of deformation, viscosity is classified as bulk or shear. Bulk viscosity manifests itself in relatively slow relaxation processes, including those connected with wave attenuation. Newton's shear viscosity is independent of the deformation rate.

Viscosity is also determined by the scale of processes involved. Low values of viscosity correspond to processes involving the generation and relaxation of dislocations. High-rate deformation at the macroscopic level is caused by increased viscosity [92].

The hydrodynamic approximation, in which strength and viscosity of solid materials are ignored, is applicable in conditions of high-intensity shock loads when the pressure greatly exceeds the shear strength of materials. Thermodynamic parameters — the pressure, temperature, and compression $\sigma = \rho/\rho_0$ (where ρ and ρ_0 are the respective densities of the compressed and original material) — are determined from the conservation laws for mass, momentum, and energy, as well as from the equation of state of the material with the kinematic parameters of the shock wave: the shock wave velocity D and the mass velocity U of matter behind the shockwave front [85]:

$$P = \rho_0 UD; \quad \sigma = \frac{D}{D-U}. \qquad (19)$$

Experimental studies [93] showed that as a result of shock compression, the state of matter behind the shockwave front becomes very nearly isotropic. However, strength properties of materials affect the process of shock compression, which deviates from the ideal liquid behavior.

A method for studying viscosity of materials behind the shockwave front was suggested by A D Sakharov in 1957 [94]. The method is based on measuring the time of evolution of harmonic perturbations created at the front of the shock wave propagating through the material under study, and then comparing the experimental results with theoretical evaluations [86]. Experimental studies were conducted at VNIIEF (the All-Russian Research Institute of Experimental Physics in Sarov) by Mineev, Oleinik, and others [86–89]; numerical processing was carried out in collaboration with Zaidel, who analyzed the effect of viscosity on the evolution of perturbations in plane shock waves [95].

Later, Miller and Ahrens [96] analyzed the method for measuring the shear viscosity suggested in [86] in more detail. They covered the effect of boundary conditions and that of the approximations chosen in [95] on the method of processing the experimental data representing the evolution

of perturbations behind the shockwave front, the method used to determine viscosity in [86–89]. The solution to the problem of propagation of perturbations given in [96], as well as that in [95], was obtained in the approximation of a Newtonian liquid with a constant viscosity independent of the loading rate. A comparison of viscosity estimates for water [88, 90] based on two approaches [95, 96] showed insignificant differences between the results and thus confirmed the reliability of data obtained in [86–89].

The plane shock wave was created in the above experiments by an explosive charge. Harmonic perturbations were generated at the arrival of the shock wave at the surface of the material under investigation. To achieve this, recesses shaped like parallel cavities of the sinusoidal profile were created on the skew surface of the wedge-shaped specimen. The distance between cavities determined the perturbation wavelength on the shockwave front. As the shock wave propagated along the wedge, the wave carrying the perturbation entered the gap between the free surface of the specimen and a plate made of a transparent material (plexiglass). Measurements of the form of the shockwave front after the shock wave has traveled along the specimen were conducted by recording the light emitted from the gap. The glow was recorded by an ultrafast photochronograph. A system of slits on the plexiglass plate permitted the determination of the wave profile at different moments of time, corresponding to the length of propagation of the shock wave along the wedge.

The pressure in the shock wave was increased by using explosive laboratory devices with spherical shock waves [97] used at VNIIEF for studying shock compression of materials. Experiments were set up in a similar way to those with a plane shock wave.

In both cases, the artificially created perturbations, characterized by a periodicity in the direction along the surface of the shockwave front, caused vibrations of matter behind the wavefront. Perturbation parameters were chosen in accordance with the selected approximation [95] that corresponded to plastic flow without taking strength parameters into account and neglecting the effect of low viscosity on the perturbation evolution,

$$\frac{Pa_0}{\lambda} > \sigma_p\,, \quad \frac{2\pi a_0}{\lambda} \ll 1\,, \tag{20}$$

where a_0 is the initial amplitude of perturbations, λ is the perturbation wavelength, P is the pressure in the shockwave, and σ_p is the dynamic yield strength. The constancy of flow behind the shockwave front, required for the calculations to correspond to the experiment, was ensured by using sufficiently large explosive charges and specimens.

The experiments studied the propagation of shock waves with different perturbation wavelengths λ at the wavefront. Complete geometric simulation of the process was carried out, including the relation $2\pi a_0/\lambda = \text{const}$.

The experimental data on the perturbation amplitude at the shockwave front as a function of the shockwave propagation length $x = s/\lambda$ (where s is the length covered by the wave) were obtained for the wavelengths $\lambda = 1.2$ and 3.3 cm and for the initial amplitudes $2\pi a_0/\lambda = 0.23-1.74$. Qualitatively, the experimental curves had the same shape as the curves calculated in [95]: the perturbation amplitude falls off, changing sign several times in the process. At the same time, it was found that the perturbation amplitude attenuation curves $a(t)/a_0$ plotted along the x axis display phase shifting for different values of the wavelength λ and of the parameter $2\pi a/\lambda$. A numerical analysis showed that this effect dominates when shear viscosity is calculated from the displacement of the point of intersection of the a/a_0 curve with the abscissa axis for various wavelengths $\Delta x = x_{02} - x_{01}$,

$$\eta = \frac{\rho D \Delta x}{k(1/\lambda_1 - 1/\lambda_2)}\,, \tag{21}$$

where ρ is the density behind the nonperturbed shockwave front and D is its wave velocity. The parameter k was found by regression analysis of the data $x_{0i} = f(1/\lambda_i, a_{0i}/\lambda_i)$ [86].

The most detailed measurements of shock compression were conducted with aluminum and lead [86, 87]. The pressure varied in the interval from 31 to 250 GPa; this range covered the regions of the solid and liquid states on the shock compression adiabat. To reveal the effect of shock heating, viscosity was also measured in porous aluminum specimens with initial density reduced by a factor of m [87]. At approximately the same pressures, the shock compression of porous specimens made it possible to achieve higher temperatures of shock compression in comparison with shock compression of nonporous specimens [98].

Figure 10 gives the phase diagram of aluminum, the shock adiabats for the nonporous ($m = 1$) and porous ($m = 1.23$, 1.43, and 4) specimens, and the results of viscosity measurements.

The aluminum melting curve was measured in [99] under static conditions on diamond anvils at pressures up to 80 GPa. At high pressures, the curve comfortably agrees with the data of theoretical calculations [100] as well as with the data on melting under shock compression obtained by measuring the speed of sound behind the shockwave front [101]. Later, first-principle calculations of the melting curve [102] also gave results close to the data in [99]. The initial region of the aluminum melting curve up to 15 GPa was confirmed by experiments [103].

Temperature estimates on shock compression adiabats in nonporous and porous specimens were obtained using the Mie–Gruneisen-type equation of state developed for metals

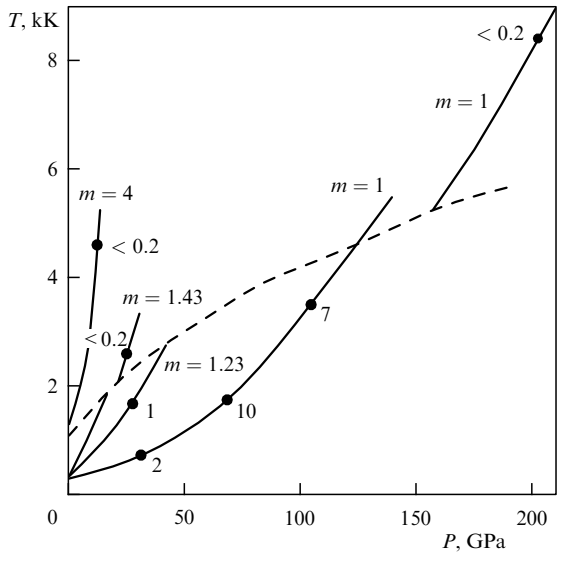

Figure 10. Aluminum melting curve (dashed line) and shock adiabats (solid curves) for different initial porosities m [99]. The numbers by the experimental points give the measured viscosity (in kPa s) [86, 87].

in [104], with separation of the lattice and electron contributions to the pressure and energy; the changes in the heat capacity and the Gruneisen coefficient were taken into account in the equation of state. Shock adiabats in the region of the liquid phase were taken from the data in [105]. The discontinuity and displacement of adiabats on the melting curves correspond to taking melting into account in shock compression calculations.

The results of viscosity measurements in aluminum under shock compression [86, 87] are shown in Fig. 10 (in kPa) by numbers near the points that correspond to the parameters of the shock waves in the experiments.

A substantial reduction in viscosity under shock compression was observed at the melting stage in the material. In the majority of measurements conducted in this field, the evolution of perturbations at the shockwave front was independent, to within experimental errors, of the perturbation wavelength, which pointed to a sharp decrease in viscosity [87]. Because the limiting resolution of recording the evolution of perturbations was $\Delta x < 0.02-0.03$, the viscosity found in [86, 87] for aluminum at $P = 202$ GPa was $\eta < 2$ kPa s; in some experiments on porous aluminum with $m = 1.43$, values $\eta < 0.2$ kPa s were observed.

Figure 11 shows a melting curve and the calculated shock adiabat for lead ($m = 1$) in the region of solid and liquid phases [106]. The melting curve was found using optical measurements of the unloading of shock-compressed lead into a transparent obstacle; as in the case of aluminum, the curve agrees with the data of static measurements [107]. The plot presents viscosity data for lead under shock compression in the solid phase region [86, 87]. Viscosity measurements at the pressures $P = 124$ and 250 GPa corresponding to temperature estimates of about 7000 and 20,000 K, i.e., above the melting curve, also manifested the behavior of perturbation evolution that was similar for different wavelengths, yielding the respective viscosity values $\eta < 30$ and 13 kPa with measurement errors taken into account.

The aluminum viscosity data in the region of the solid phase are described in [87] on the basis of the activation model

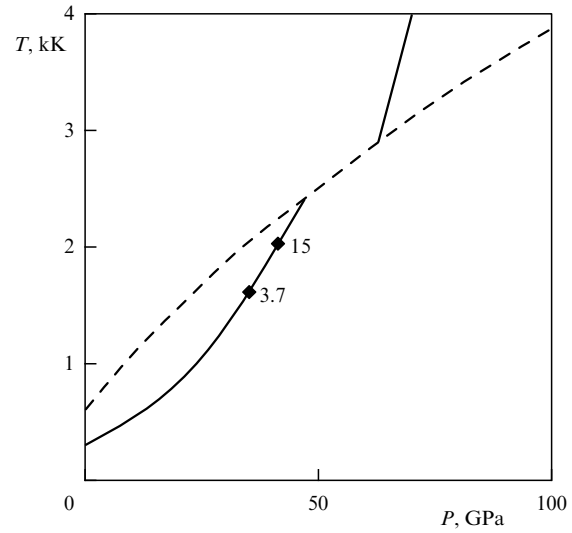

Figure 11. Melting curve (dashed line) and shock adiabats (solid lines) for lead at $m = 1$ [106]. Numbers at the experimental points show the measured values of viscosity (in kPa s) [87].

[35, 36]. For this, the viscosity was written as

$$\eta(\delta, T) = \eta_0 \sigma \exp \frac{E_{\text{act}}(\sigma)}{RT} . \tag{22}$$

This representation of the temperature dependence of viscosity was used for describing experimental data for liquid metals and molten alloys at normal pressure, along with other forms of dependence, including that given in [108]. However, as we mentioned earlier, relation (22) is not substantially different from the classic formula (5) chosen owing to the structural similarity of liquid and solid bodies in the vacancy model of thermal atomic motion.

The function chosen in [87] on the basis of qualitative arguments was

$$E_{\text{act}}(\sigma) = a + b\sigma^m . \tag{23}$$

However, calculations failed to establish physically acceptable values of the constants a and b.

Relation (22) was also used successfully in [109] to describe aluminum and lead viscosity data in [86, 87] on the shock adiabat of nonporous materials ($m = 1$) in the regions of solid and liquid phases. The values of $E_{\text{act}}(\sigma)$ were found from experimental data by inverting (22) as

$$E_{\text{act}}(\sigma) = T\left(\frac{\ln \eta}{\eta_0} - \ln \sigma\right) . \tag{24}$$

It was assumed that $E_{\text{act}}(\sigma)$ must be a monotonically increasing function corresponding to the totality of the data within the experimental errors. Numerical estimates showed that in this case, $E_{\text{act}}(\sigma)$ is a step function that can be written as

$$E_{\text{act}}(\sigma) = a + b \text{ th}\big[c(\sigma - d)\big] . \tag{25}$$

Numerical values of the parameters in Eqn (25) were found from the condition of the minimal least-square deviation of the obtained values of $E_{\text{act}}(\sigma)$. The initial values of viscosity at $P = 0.1$ MPa were taken from [110]. Close to them are the data on aluminum and lead viscosity obtained in the pressure range 0.1 – 5 GPa in [111 – 113]. The calculated data in [109], converted to the viscosity as a function of pressure, plus the viscosity data on adiabats of shock compression of aluminum and lead, are plotted in Fig. 12.

The calculated curves $\eta(P)$ in Fig. 12 correspond to the activation energies 2.1 and 56 kJ mole^{-1} for aluminum and 4.2 and 60 kJ mole^{-1} for lead on the initial rising branch and the subsequent falling branch, respectively. This considerable change in the activation energy under shock compression corresponds to the fact that the growth of pressure at the initial stage, corresponding mostly to cold compression, is accompanied by a slight increase in temperature.

As the pressure grows, the contribution of thermal pressure increases. The growth of the internal energy and temperature with increasing the pressure in the region of the liquid state is substantially steeper than that of cold compression of the specimen [104]. Thus, the share of the thermal energy of aluminum and lead in the shock compression energy at $P = 200$ GPa is about 60 and 35%, respectively. According to estimates obtained using the equation of state in [60], the share of thermal energy at the same pressure in compressed iron was 54%. Therefore, as the pressure grows in the region of liquid state of a metal under shock compression, its viscosity must decrease in response to increasing the temperature.

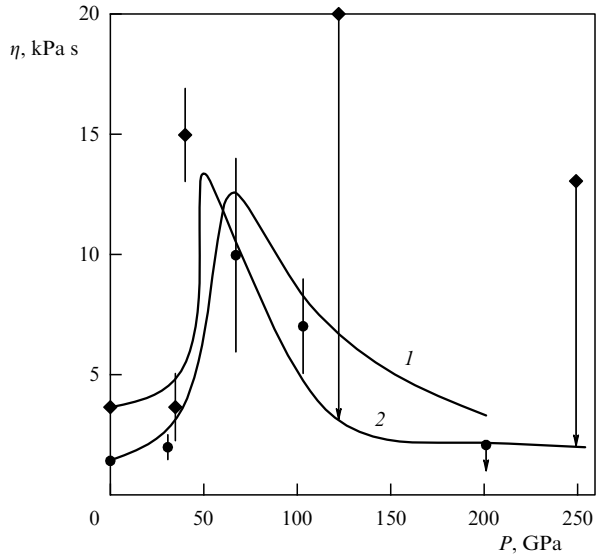

Figure 12. Viscosity of aluminum and lead on shock adiabats ($m = 1$): • — aluminum, ◆ — lead; *1*, *2* — calculated curves based on data from [109] for aluminum and lead, respectively.

Isolated measurements of viscosity in [86] by the method of the progress of perturbations at the shockwave front in iron at $P = 39$ GPa gave values close to the aluminum viscosity in the same pressure range. Although no measurements were conducted in iron at higher pressures, we can expect that its viscosity under shock compression should manifest a behavior similar to that observed in aluminum and lead.

It must be mentioned that the method of measuring viscosity by monitoring the evolution of harmonic perturbations at the shockwave front corresponds to the viscosity effects in the region of flow behind the front where the relaxation of mobile dislocations is already complete and their concentration, according to the estimates in [114], reaches $10^7 - 10^8$ cm^{-2}, while more than 10^9 cm^{-2} of dislocations form at the front of the shock wave. The deformation and its rate behind the shockwave front are given by

$$\varepsilon = \frac{2\pi a_0}{\lambda}\ , \quad \frac{\mathrm{d}\varepsilon}{\mathrm{d}t} = \frac{4\pi^2 a_0 D}{\lambda^2}\ . \tag{26}$$

The deformation rate in viscosity measurements in aluminum at $P = 31$ GPa, carried out in [87], was $\sim 10^7$ s^{-1}, and in [86] it varied from 4×10^5 to 8×10^6 s^{-1}. As we see from Fig. 12, viscosity values in the pressure range up to ~ 30 GPa, where shock heating is not very high, remained nearly constant and independent of the deformation rate, that is, viscosity was Newtonian. The values of viscosity in this range of pressure were found not to be very different in aluminum and lead. As the pressure on the shock adiabat increased in the range $P = 50 - 100$ GPa, the viscosity grew to $\eta \sim 10 - 15$ kPa s.

Under conditions of dynamic loading at lower deformation rates $\mathrm{d}\varepsilon/\mathrm{d}t = 6 \times 10^2 - 6 \times 10^3$ s^{-1}, nearly equal values $\eta = (3-4) \times 10^4$ Pa s were found in [115, 116] in aluminum and various grades of steel. The viscosities of aluminum and steel were also very close in the range $\mathrm{d}\varepsilon/\mathrm{d}t > 10^4$ s^{-1}, and were only slightly affected by the deformation rate [113]. The initial increase and the subsequent decrease in the aluminum viscosity with increasing the pressure was also observed in [117] at deformation rates $\mathrm{d}\varepsilon/\mathrm{d}t > 10^5$ s^{-1}.

The viscosity obtained in measurements of the shockwave front width at pressures of shock compression of 41 and 139 GPa in aluminum and steel [114] corresponded to a deformation rate of 7×10^7 s^{-1} and reached 10^2 and 4×10^2 Pa s.

As pointed out in [109], the drop in viscosity in the region of transition to melting on the shock adiabat is similar to a change in the yield strength [118 – 120] and in the spalling strength [121].

The change in viscosity under shock compression is thus caused by competing processes of compression and heating of matter; it is determined by the transition from the solid to liquid state.

7. Conclusion

The results of measuring viscosity in the vicinity of the iron melting curve at pressures up to 10 – 20 GPa correspond to the values $\sim (0.5-1.5) \times 10^{-2}$ Pa s and approximately coincide with the measurement data for iron – sulfur melts that constitute the likely composition of the earth's outer core.

The calculated values of the molecular shear viscosity in the pressure range up to ~ 5 GPa are consistent with the measurement results.

The calculations of shear viscosity of iron at the boundaries of the earth's outer core at 130 and 330 GPa yield values $\sim (1-1.5) \times 10^{-2}$ Pa s. Because both groups of data correspond to states near the melting curve, this contradicts both the hypothesis of a considerable rise in viscosity with increasing the pressure and the hypothesis of a glassy state of the earth's inner core.

According to the measurement results of viscosity of metals under shockwave conditions, a considerable drop in viscosity is observed after melting on the shock adiabat.

The differences between estimates of the viscosity variation along the melting curve of iron in the pressure range typical of the earth's outer core point to a serious problem in extrapolating the experimental data in terms of the available model concepts, including the Arrhenius activation model.

The complicated nonmonotonic and ambiguous behavior of the melting curve of iron that is revealed in static and dynamic measurements makes it difficult to extrapolate viscosity to the range of high pressures characterizing the earth's core.

References

1. Brazhkin V V, Lyapin A G *Usp. Fiz. Nauk* **170** 535 (2000) [*Phys. Usp.* **43** 493 (2000)]
2. Gutenberg B *Physics of the Earth's Interior* (New York: Academic Press, 1959) [Translated into Russian (Moscow: IL, 1963)]
3. Dziewonski A M, Anderson D L *Phys. Earth Planet. Inter.* **25** 297 (1981)
4. Mao H K et al. *J. Geophys. Res.* **95** 21737 (1990)
5. Poirier J-P *Phys. Earth Planet. Inter.* **85** 319 (1994)
6. Boehler R *Rev. Geophys.* **38** (2) 221 (2000)
7. Jacobs J A *The Earth's Core* (London: Academic Press, 1975) [Translated into Russian (Moscow: Mir, 1979)]
8. Brazhkin V V *Pis'ma Zh. Eksp. Teor. Fiz.* **68** 469 (1998) [*JETP Lett.* **68** 502 (1998)]
9. Bridgman P W *Collected Experimental Papers* Vol. IV (Cambridge, Mass.: Harvard Univ. Press, 1964) p. 2155
10. LeBlanc G E, Secco R A *Geophys. Res. Lett.* **23** 213 (1996)
11. Vočadlo L et al. *Faraday Discuss.* **106** 205 (1997)
12. De Wijs G A et al. *Nature* **392** 805 (1998)
13. Alfè D, Gillan M J *Phys. Rev. B* **58** 8248 (1998)
14. Alfè D, Gillan M *Phys. Rev. Lett.* **81** 5161 (1998)

15. Alfè D, Kresse G, Gillan M J *Phys. Rev. B* **61** 132 (2000)
16. Zhang Y, Guo G, Nie G *Phys. Chem. Minerals* **27** 164 (2000)
17. Laio A et al. *Science* **287** 1027 (2000)
18. Vočadlo L et al. *Phys. Earth Planet. Inter.* **120** 145 (2000)
19. Zhang J-G, Guo G-J *Phys. Earth Planet. Inter.* **122** 289 (2000)
20. Belonoshko A B, Ahuja R, Johansson B *Phys. Rev. Lett.* **84** 3638 (2000)
21. Dobson D P *Phys. Earth Planet. Inter.* **130** 271 (2002)
22. Dobson D P *Phys. Earth Planet. Inter.* **120** 137 (2000)
23. Rutter M D et al. *Phys. Rev. B* **66** 060102(R) (2002)
24. Urakawa S et al. *Am. Mineral.* **86** 578 (2001)
25. Terasaki H et al. *Earth Planet. Sci. Lett.* **190** 93 (2001)
26. Rutter M D et al. *Geophys. Res. Lett.* **29** (8) 58-1 (2002)
27. Dobson D P et al. *Am. Mineral.* **85** 1838 (2000)
28. Terasaki H et al. *Geophys. Res. Lett.* **29** (8) 68-1 (2002)
29. Dingwell D B *Rev. Mineral.* **37** 397 (1999)
30. Brazhkin V V, Popova S V *Rasplavy* (4) 97 (1989)
31. Brazhkin V V, Voloshin R N, Popova S V *Rasplavy* (1) 10 (1990)
32. Mungall J E *Geochim. Cosmochim. Acta* **66** (1) 125 (2002)
33. Poirier J P *Geophys. J.* **92** 99 (1988)
34. Urakawa S et al. *Rev. High Pressure Sci. Technol.* **7** 286 (1998)
35. Frenkel' Ya I *Kinematicheskaya Teoriya Zhidkosteĭ* (Kinetic Theory of Liquids) (Moscow – Leningrad: Izd. AN SSSR, 1945) [Translated into English (Oxford: The Clarendon Press, 1946)]
36. Glasstone S, Laidler K J, Eyring H *The Theory of Rate Processes* (New York: McGraw-Hill Book Co., 1941) [Translated into Russian (Moscow: IL, 1948)]
37. Cohen M N, Turnbull D *J. Chem. Phys.* **31** 1164 (1959)
38. Swalin R A *Acta Metall.* **7** 736 (1959)
39. Nahtrieb N *Adv. Phys.* **16** 309 (1967)
40. Arsent'ev P P, Koledov L A *Metallicheskiye Rasplavy i Ikh Svoĭstva* (Metallic Melts and Their Properties) (Moscow: Metallurgiya, 1976)
41. Frenkel' Ya I *Vvedenie v Teoriyu Metallov* (Introduction to the Theory of Metals) 3rd ed. (Moscow: Fizmatgiz, 1958)
42. Boehler R *Earth Planet. Sci. Lett.* **111** 217 (1992)
43. Boehler R *Phys. Earth Planet. Inter.* **96** 181 (1996)
44. Anderson O L *J. Geophys. Res.* **95** (B13) 21697 (1990)
45. Andrault D et al. *Am. Mineral.* **85** 364 (2000)
46. Sanloup C F et al. *Europhys. Lett.* **52** 151 (2000)
47. Lucas L D *CR Acad. Sci.* **259** 3760 (1964)
48. Yang L, Simnad M T, Derge G *J. Met. Soc. Am.* **206** 1577 (1956)
49. Anderson O L, Isaak D G *Phys. Earth Planet. Inter.* **131** 19 (2002)
50. Kuskov O L, Khitarov N I *Termodinamika i Geokhimiya Yadra i Mantii Zemli* (Thermodynamics and Geochemistry of the Earth's Core and Mantle) (Moscow: Nauka, 1982)
51. Sherman D M *Earth Planet. Sci. Lett.* **153** 149 (1997)
52. Anderson W W, Ahrens T J *J. Geophys. Res.* **101** (B3) 5627 (1996)
53. Boehler R *Nature* **363** 534 (1993)
54. Saxena S K, Shen G, Lazor P *Science* **260** 1312 (1993)
55. Saxena S K et al. *Science* **269** 1703 (1995)
56. Yoo C S et al. *Science* **270** 1473 (1995)
57. Andrault D et al. *Science* **278** 831 (1997)
58. Shen G et al. *Geophys. Res. Lett.* **25** (3) 373 (1998)
59. Ahrens T J, Holland K G, Chen G Q *Geophys. Res. Lett.* **29** (7) 54 (2002)
60. Funtikov A I *Teplofiz. Vys. Temp.* **41** 954 (2003) [*High Temp.* **41** 850 (2003)]
61. Errandonea D et al. *Phys. Rev. B* **63** 132104 (2001)
62. Brown J M, McQueen R G *J. Geophys. Res.* **91** 7485 (1986)
63. Nguyen J H, Holms N C, in *Science and Technology of High Pressure*: *Proc. of the Intern. Conf. on High Pressure Science and Technology* (*AIRAPT–17*), *Honolulu, Hawaii, 25–30 July 1999* (Eds M H Manghnani, W J Nellis, M F Nicol) (Hyderabad: Univ. Press (India), 2000) p. 156
64. Ahrens T J, Hua Tan, Bass J D *High Pressure Res.* **2** 145 (1990)
65. Yoo C S et al. *Phys. Rev. Lett.* **70** 3931 (1993)
66. Funtikov A I, Osipov R S, Tsyganov V A *Teplofiz. Vys. Temp.* **37** 887 (1999) [*High Temp.* **37** 857 (1999)]
67. Anderson O L, Isaak D G *Am. Mineral.* **85** 376 (2000)
68. Zharkov V N *Vnutrennee Stroenie Zemli i Planet* (Interior Structure of the Earth and Planets) 2nd ed. (Moscow: Nauka, 1983) [Translated into English (Chur: Harwood Acad. Publ., 1986)]
69. Anderson D L *Nature* **285** 204 (1980)
70. Stevenson D J *J. Geophys. Res.* **88** 2445 (1983)
71. Cormier V F *Phys. Earth Planet. Inter.* **24** 291 (1981)
72. Courtier N et al. *Phys. Earth Planet. Inter.* **117** 3 (2000)
73. Smylie D E, McMillan D G *Phys. Earth Planet. Inter.* **117** 71 (2000)
74. Rieutord M *Phys. Earth Planet. Inter.* **131** 269 (2002)
75. Greff-Lefftz M, Legros H, Dehant V *Phys. Earth Planet. Inter.* **122** 187 (2000)
76. Vočadlo L et al. *Geophys. Res. Lett.* **26** 1231 (1999)
77. Alfè D, Gillan M J, Price G D *Nature* **401** 462 (1999)
78. Gans R F *J. Geophys. Res.* **77** (B2) 360 (1972)
79. Svendsen B et al. *Phys. Earth Planet. Inter.* **55** 154 (1989)
80. Stixrude L, Cohen R E, Hemley R J *Rev. Mineral.* **37** 639 (1998)
81. Alfè D, Gillan M J *Phys. Rev. Lett.* **81** 5161 (1998)
82. Funtikov A I *Fizika Zemli* **37** (9) 3 (2001) [*Izv., Phys. Solid Earth* **37** 703 (2001)]
83. Funtikov A I *Fizika Zemli* **36** (11) 70 (2000) [*Izv., Phys. Solid Earth* **36** 958 (2000)]
84. Anderson O L *Geophys. J. R. Astron. Soc.* **84** 561 (1986)
85. Al'tshuler L V *Usp. Fiz. Nauk* **85** (2) 197 (1965) [*Sov. Phys. Usp.* **8** 52 (1965)]
86. Sakharov A D et al. *Dokl. Akad. Nauk SSSR* **159** 1019 (1964)
87. Mineev V N, Savinov E V *Zh. Eksp. Teor. Fiz.* **52** 629 (1967) [*Sov. Phys. JETP* **25** 411 (1967)]
88. Mineev V N, Zaidel P M *Zh. Eksp. Teor. Fiz.* **54** 1633 (1968) [*Sov. Phys. JETP* **27** 874 (1968)]
89. Mineev V N, Savinov Ye V *Zh. Eksp. Teor. Fiz.* **68** 1321 (1975) [*Sov. Phys. JETP* **41** 656 (1975)]
90. Al'tshuler L V, Kanel' G I, Chekin B S *Zh. Eksp. Teor. Fiz.* **72** 663 (1977) [*Sov. Phys. JETP* **45** 348 (1977)]
91. Kanel' G I, Razorenov S V, Utkin A V, Fortov V E *Udarno-Volnovye Yavleniya v Kondensirovannykh Sredakh* (Shockwave Phenomena in Condensed Media) (Moscow: Yanus-K, 1996); see also Kanel S I , Razorenov S V, Fortov V E *Shock-Wave Phenomena and the Properties of Condensed Matter* (New York: Springer, 2004)
92. Savenkov G G, Meshcheryakov Yu I *Fiz. Goreniya Vzryva* **36** (3) 113 (2002)
93. Dremin A N, Kanel' G I *Prikl. Mekh. Tekh. Fiz.* (2) 146 (1976)
94. Al'tshuler L V et al *Usp. Fiz. Nauk* **169** 323 (1999) [*Phys. Usp.* **42** 261 (1999)]
95. Zaidel P M *Prikl. Mekh. Tekh. Fiz.* (4) 30 (1967)
96. Miller G H, Ahrens T J *Rev. Mod. Phys.* **63** 919 (1991)
97. Al'tshuler L V et al. *Usp. Fiz. Nauk* **166** 575 (1996) [*Phys. Usp.* **39** 539 (1996)]
98. Zel'dovich Ya B, Raĭzer Yu P *Fizika Udarnykh Voln i Vysokotemperaturnykh Gidrodinamicheskikh Yavleniĭ* (Physics of Shock Waves and High-Temperature Hydrodynamic Phenomena) (Moscow: Fizmatgiz, 1963) [Translated into English (New York: Academic Press, 1967)]
99. Boehler R, Ross M *Earth Planet. Sci. Lett.* **153** 223 (1997)
100. Moriarty J A, Young D A, Ross M *Phys. Rev. B* **30** 578 (1984)
101. Shaner J W, Brown R G, McQueen R G, in *High Pressure in Science and Technology*: *Proc. of the 9th AIRAPT Intern. High Pressure Conf., New York, USA, July 24–29, 1983* (Mater. Res. Soc. Symp. Proc., Vol. 22, Eds C Homan, R K MacCrone, E Whalley) (New York: North-Holland, 1984) p. 137
102. Vočadlo L, Alfè D *Phys. Rev. B* **65** 214105 (2002)
103. Asay J R, Hayes D B *J. Appl. Phys.* **46** 4789 (1975)
104. Kormer S B et al. *Zh. Eksp. Teor. Fiz.* **42** 686 (1962) [*Sov. Phys. JETP* **15** 477 (1962)]
105. Kopyshev V P, Medvedev A I *Termodinamicheskaya Model' Szhimaemogo Kovolyuma* (Thermodynamic Model of Compressible Covolume) (Sarov: RFYaTs-VNIIEF, 1995)
106. Mabire C, Hereil P L, in *Shock Compression of Condensed Matter, 2001* (AIP Conf. Proc., Vol. 620, Eds M D Furnish, N N Thadhani, Y Horie) (Melville, NY: AIP, 2002) p. 229
107. Godwal B K et al. *Science* **248** 462 (1990)
108. Andrade E N *Proc. R. Soc. London Ser. A* **215** 36 (1952)
109. Ogorodnikov V A et al. *Prikl. Mekh. Tekh. Fiz.* (5) 5 (1995) [*J. Appl. Mech. Tech. Phys.* **36** 438 (1995)]
110. Stepanov G V *Uprugoplasticheskoe Deformirovanie i Razrushenie Materialov pri Impul'snom Nagruzhenii* (Elastoplastic Deformation and Breakdown of Materials under Pulsed Loading) (Kiev: Naukova Dumka, 1991)

111. Zakharenko I D, Mali V I, in *Gorenie i Vzryv*: *Materialy 3-go Vsesoyuz. Simp., Leningrad, 5 – 10 Iyulya 1971 g.* (Burning and Explosion: Proc. of 3rd USSR Symp., Leningrad, 5 – 10 July 1971) (Moscow: Nauka, 1972) p. 575
112. Deribas A A *Fizika Uprochneniya i Svarki Vzryvom* (Physics of Strengthening and Explosive Welding) (Novosibirsk: Nauka, 1980)
113. Godunov S K et al. *Fiz. Goreniya Vzryva* (1) 135 (1971)
114. Chhabildas L C, Asay J R *J. Appl. Phys.* **50** 2749 (1979)
115. Ilyushin A A *Uchenye Zapiski Mosk. Gos. Univ., Mekh.* **39** 11 (1940)
116. Popov S M *Inzhenernyĭ Sbornik* **1** 27 (1941)
117. Stepanov G V, Kharchenko V V *Probl. Prochnosti* (8) 59 (1985)
118. Bat'kov Yu V, Glushak B L, Novikov S A *Fiz. Goreniya Vzryva* (5) 126 (1989)
119. Bat'kov Yu V et al. *Prikl. Mekh. Tekh. Fiz.* (1) 149 (1988)
120. Chhabildas L C, Furnish M D, Reinhart W D, in *Shock Compression of Condensed Matter – 1999* (AIP Conf. Proc., Vol. 505, Eds M D Furnish, L C Chhabildas, R S Hixson) (Melville, NY: AIP, 2000) p. 97
121. Ogorodnikov V A et al. *Fiz. Goreniya Vzryva* (1) 94 (1992) [*Cembust. Explosion Shock Waves* **28** 88 (1992)]